

## Electronic supplementary information

# Crystallographic interface control of the plasmonic photocatalyst consisting of gold nanoparticles and titanium(IV) oxide

*Shin-ichi Naya,<sup>a</sup> Atsunobu Akita,<sup>b</sup> Yoko Morita,<sup>b</sup> Musashi Fujishima,<sup>b,c</sup>  
and Hiroaki Tada<sup>\*b,c</sup>*

<sup>a</sup> Environmental Research Laboratory, Kindai University, 3-4-1, Kowakae, Higashi-Osaka, Osaka 577-8502, Japan.

<sup>b</sup> Graduate School of Science and Engineering, Kindai University, 3-4-1, Kowakae, Higashi-Osaka, Osaka 577-8502, Japan.

<sup>c</sup> Department of Applied Chemistry, Faculty of Science and Engineering, Kindai University, 3-4-1, Kowakae, Higashi-Osaka, Osaka 577-8502, Japan.

\* To whom correspondence should be addressed: TEL: +81-6-6721-2332, FAX: +81-6-6727-2024,  
E-mail: [h-tada@apch.kindai.ac.jp](mailto:h-tada@apch.kindai.ac.jp).

## **Table of contents**

- |                                   |        |
|-----------------------------------|--------|
| 1.     Supplementary Figures..... | S3-11  |
| 2.     Supplementary Tables.....  | S12-16 |

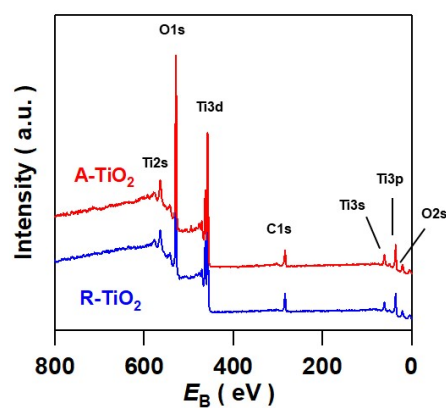


**Fig. S1.** Wide-scan XP spectra of anatase TiO<sub>2</sub> (A-TiO<sub>2</sub>) and rutile TiO<sub>2</sub> (R-TiO<sub>2</sub>).

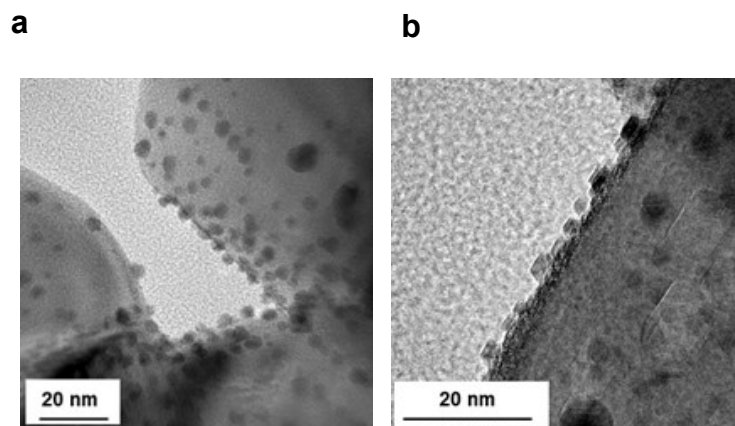


**Fig. S2.** TEM images of Au/A-TiO<sub>2</sub> (a) and Au/R-TiO<sub>2</sub> (b).

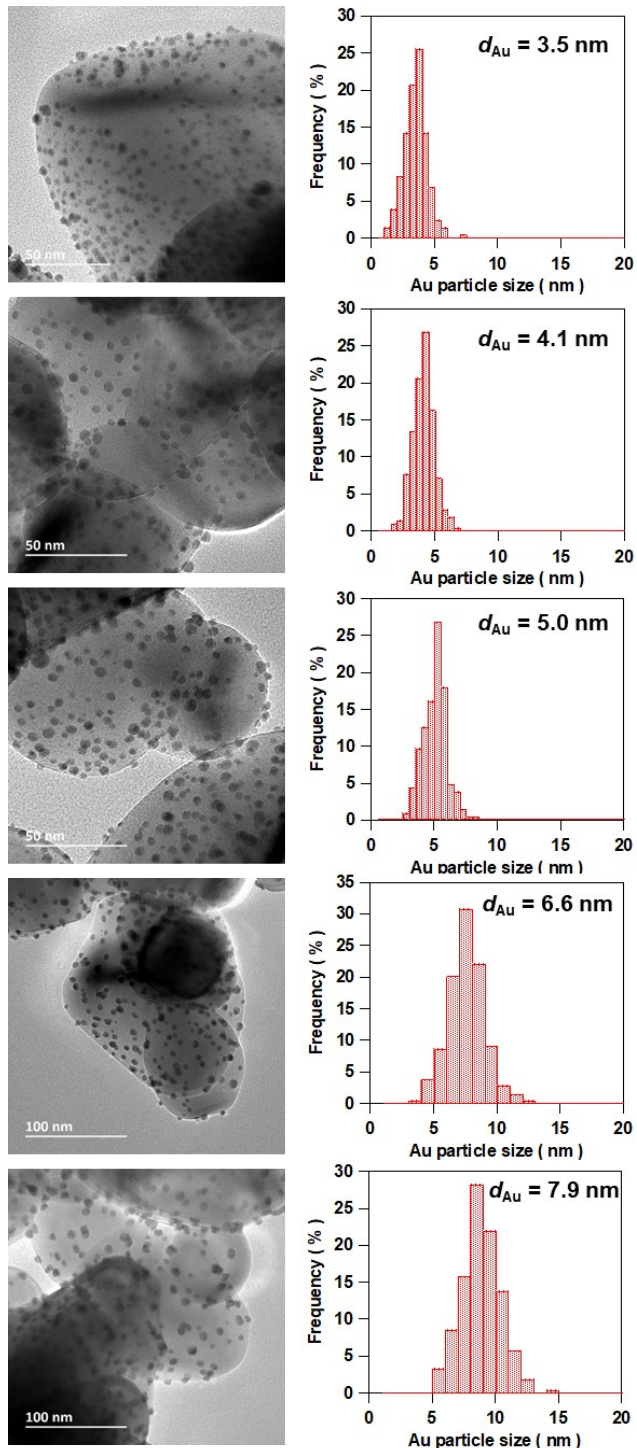


**Fig. S3.** TEM images and Au size distributions of Au/A-TiO<sub>2</sub> prepared by the deposition precipitation under different conditions.

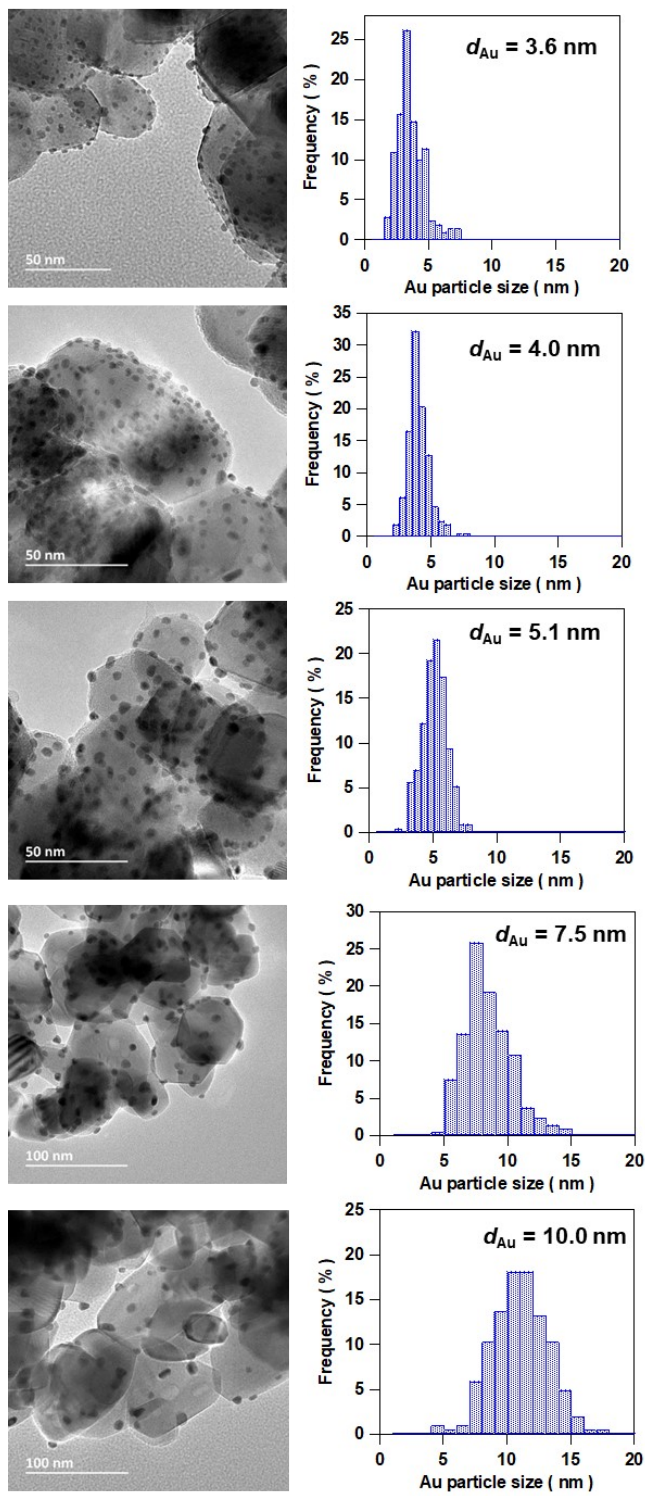


**Fig. S4.** TEM images and Au size distributions of Au/R-TiO<sub>2</sub> prepared by the deposition precipitation under different conditions.

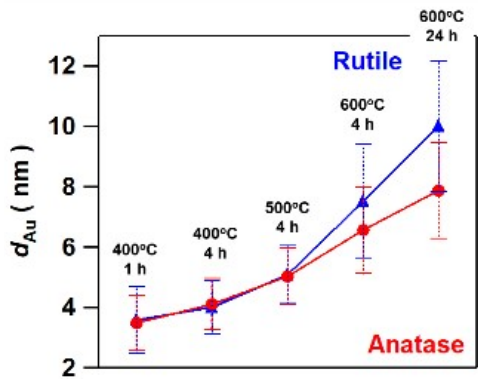


**Fig. S5.** Au particle size control on anatase and rutile  $TiO_2$  particles. The calcination temperature and time of  $Au/TiO_2$  are shown above each data point.

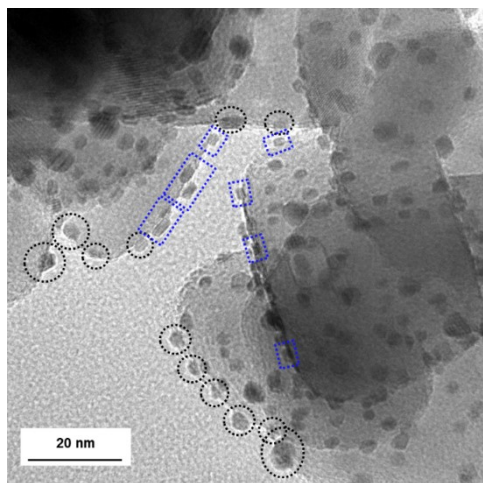


**Fig. S6.** TEM image of  $Au/R-TiO_2$  prepared at  $T_c = 673$  K and  $t_c = 1$  h. Faceted and non-faceted Au NPs are shown by dotted blue rectangle and black circle.

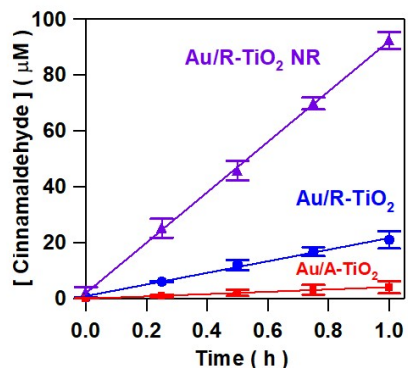
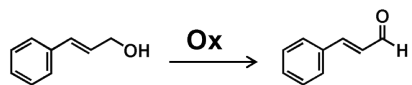


**Fig. S7.** Time courses for cinnamyl alcohol oxidation under visible-light irradiation ( $\lambda_{\text{ex}} > 490$  nm, light intensity integrated from 420 to 485 nm = 3.3 mW cm<sup>-2</sup>) in the presence of Au/A-TiO<sub>2</sub> or Au/R-TiO<sub>2</sub> or Au/R-TiO<sub>2</sub> NR.

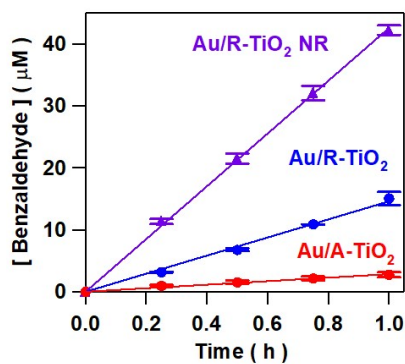
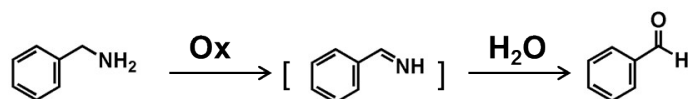


**Fig. S8.** Time courses for benzylamine oxidation under visible-light irradiation ( $\lambda_{\text{ex}} > 430$  nm, light intensity integrated from 420 to 485 nm = 6.0 mW cm<sup>-2</sup>) in the presence of Au/A-TiO<sub>2</sub> or Au/R-TiO<sub>2</sub> or Au/R-TiO<sub>2</sub> NR.

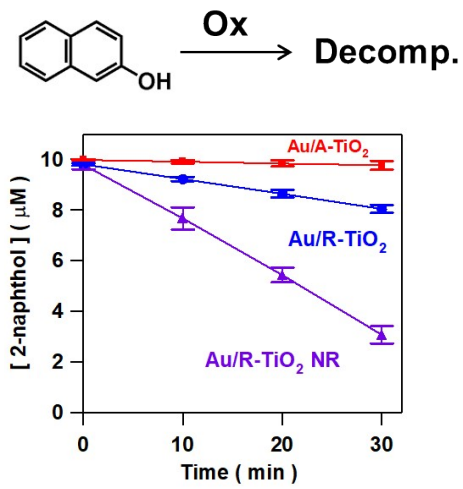


**Fig. S9.** Time courses for 2-naphthol decomposition under visible-light irradiation ( $\lambda_{\text{ex}} > 430$  nm, light intensity integrated from 420 to 485 nm = 6.0 mW cm<sup>-2</sup>) in the presence of Au/A-TiO<sub>2</sub> or Au/R-TiO<sub>2</sub> or Au/R-TiO<sub>2</sub> NR.

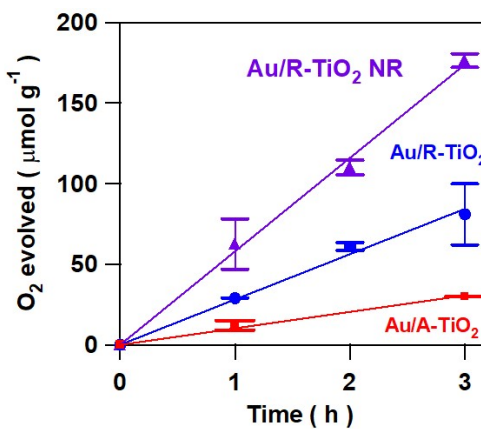
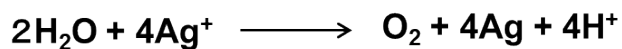


**Fig. S10.** Time courses for O<sub>2</sub> evolution from 10 mM aqueous solution of AgNO<sub>3</sub> (10 mL) containing La<sub>2</sub>O<sub>3</sub> (20 mg) under visible-light irradiation ( $\lambda_{\text{ex}} > 470$  nm, light intensity = 30 mW cm<sup>-2</sup>) in the presence of Au/A-TiO<sub>2</sub> or Au/R-TiO<sub>2</sub> or Au/R-TiO<sub>2</sub> NR (10 mg).

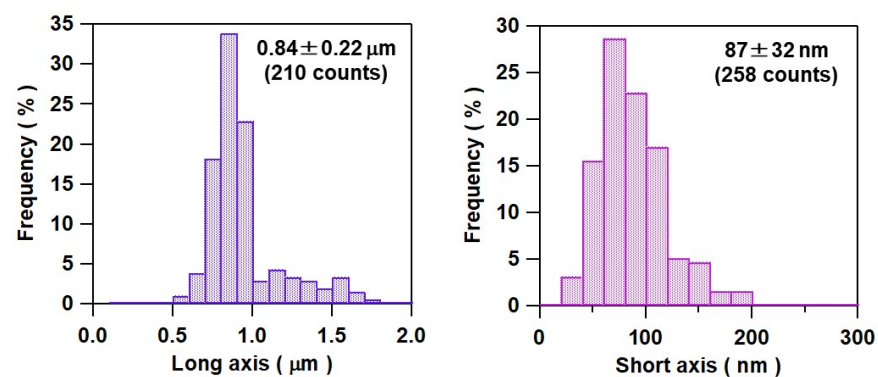
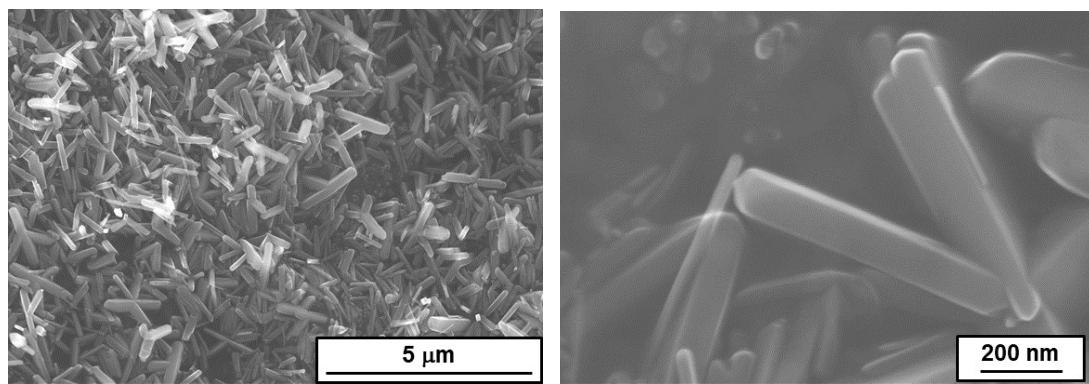


**Fig. S11.** SEM images and distribution of long and short axis length of R-TiO<sub>2</sub> NR.

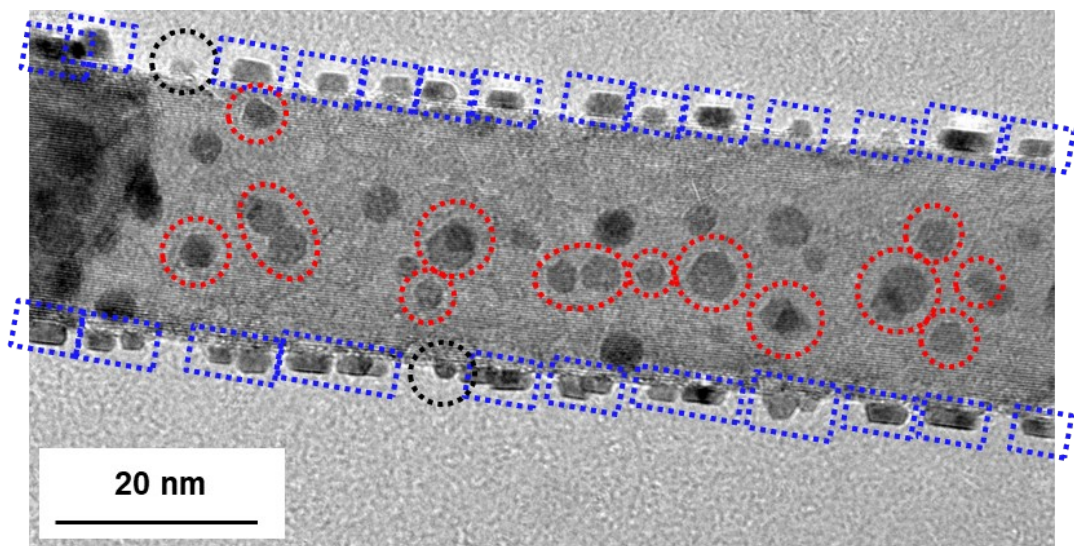


**Fig. S12.** TEM image of Au/R-TiO<sub>2</sub> NR prepared at  $T_c = 673$  K and  $t_c = 1$  h. Faceted and non-faceted Au NPs are shown by dotted blue rectangle and black circle.

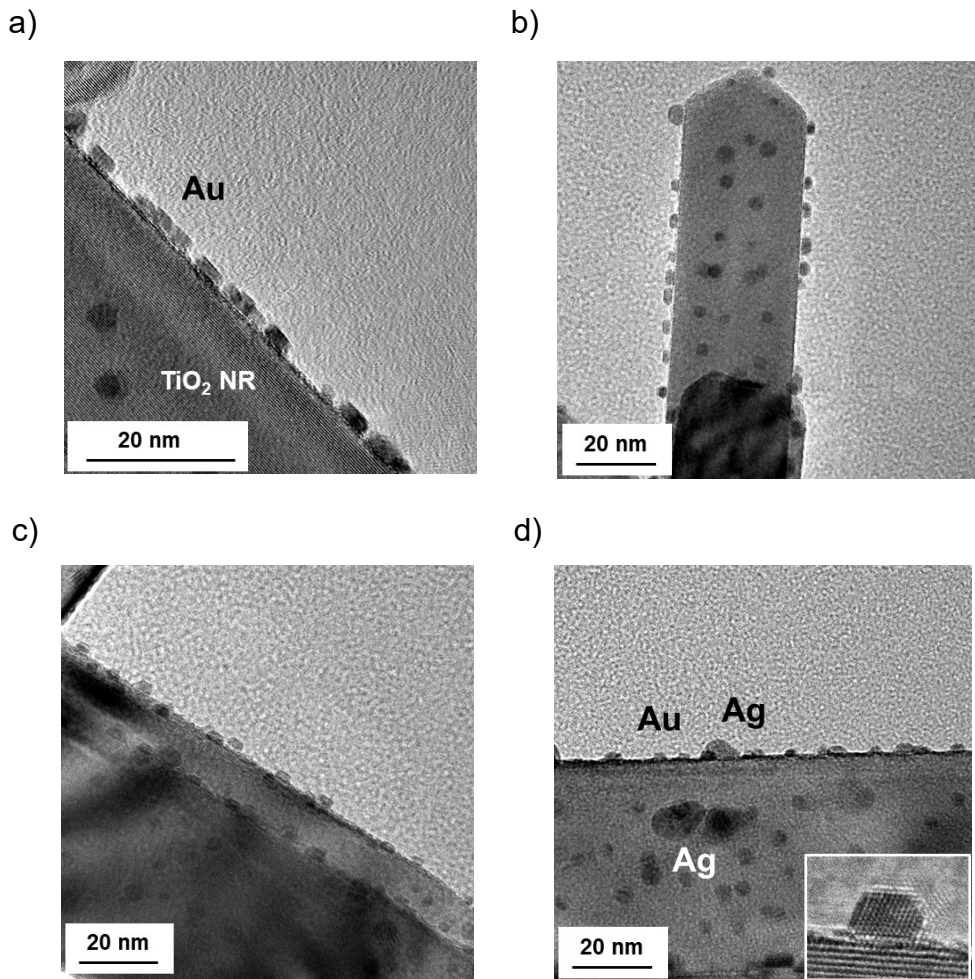


**Fig. S13.** TEM images of Au/R-TiO<sub>2</sub> NR after reactions: (a) the oxidations of cinnamyl alcohol to cinnamaldehyde, (b) benzylamine to benzaldehyde, (c) the oxidative degradation of 2-naphthol, and (d) O<sub>2</sub> evolution from 10 mM aqueous solution of AgNO<sub>3</sub>.

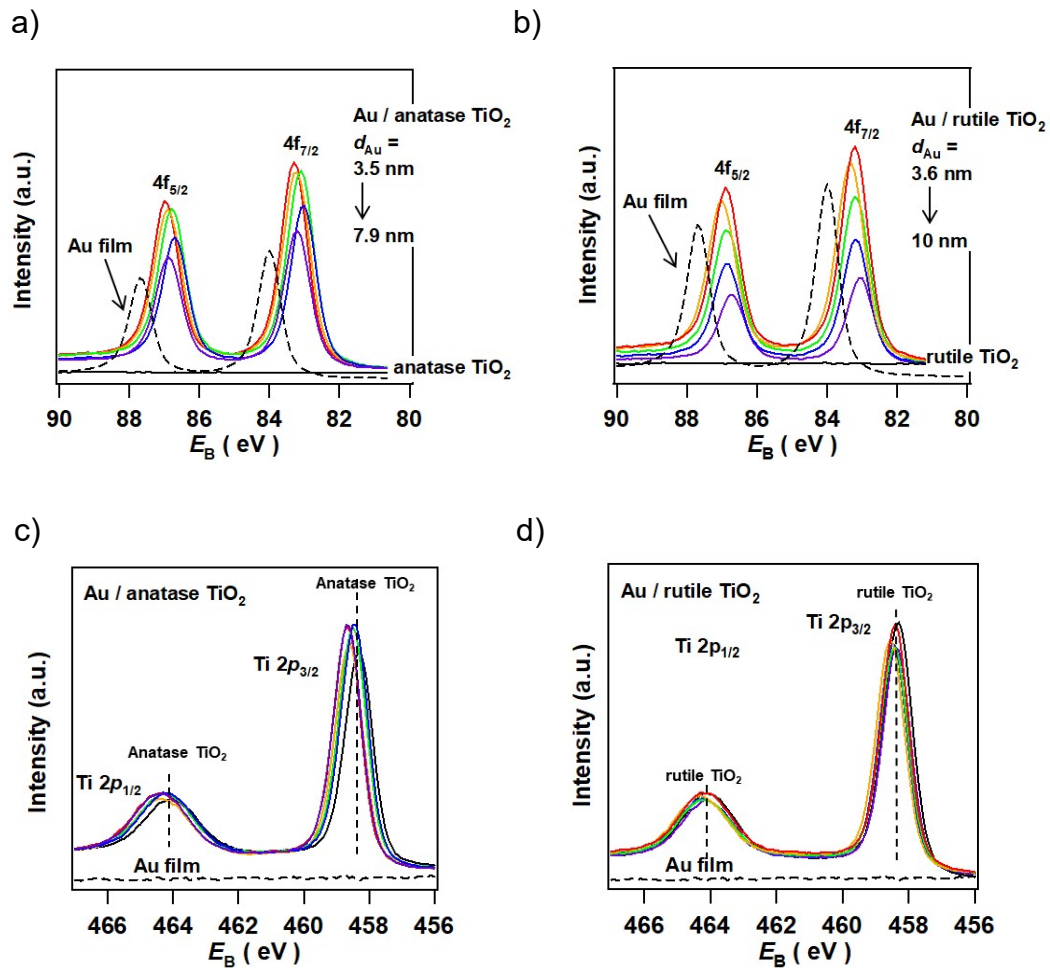


**Fig. S14.** Au 4f-XP spectra of Au/A- $\text{TiO}_2$  (a) and Au/R- $\text{TiO}_2$  (b) with varying  $d_{\text{Au}}$ , and unmodified  $\text{TiO}_2$  and Au film-coated glass plate for comparison. Ti 2p-XP spectra of Au/A- $\text{TiO}_2$  (c) and Au/R- $\text{TiO}_2$  (d) with varying  $d_{\text{Au}}$ , and unmodified  $\text{TiO}_2$  and Au film-coated glass plate for comparison.

**Table S1.** Crystal-form effect on the plasmonic photocatalytic activity of Au/TiO<sub>2</sub>

Reaction	Reaction rate		ratio of R/A	Ref.
	Rutile (R)	Anatase (A)		
2-Propanol oxidation	0.545 μmol h <sup>-1</sup>	0.284 μmol h <sup>-1</sup>	1.96	S1,2
Cinnamyl alcohol oxidation	6.00 μmol h <sup>-1</sup>	1.03 μmol h <sup>-1</sup>	5.81	S3
Benzylamine oxidation	1.82 μmol h <sup>-1</sup>	0.102 μmol h <sup>-1</sup>	17.8	S4
H <sub>2</sub> evolution	18.5 μmol h <sup>-1</sup>	0 μmol h <sup>-1</sup>	---	S5
Nitrobenzene reduction	7.38 μmol h <sup>-1</sup>	1.04 μmol h <sup>-1</sup>	7.10	S6
Oxygen evolution reaction	10.1 μmol h <sup>-1</sup>	2.24 μmol h <sup>-1</sup>	4.52	S7
Water oxidation	4.46 μA cm <sup>-2</sup>	0.109 μA cm <sup>-2</sup>	40.9	S8
Nonylphenol degradation	2.46 μmol h <sup>-1</sup>	0.321 μmol h <sup>-1</sup>	7.65	S9
2-Naphthol degradation	2.40 μmol h <sup>-1</sup>	0.238 μmol h <sup>-1</sup>	10.1	S10

**Reference**

- (S1) E. Kowalska, R. Abe and B. Ohtani, Visible light-induced photocatalytic reaction of gold-modified titanium(IV) oxide particles: action spectrum analysis. *Chem. Commun.*, 2009, **45**, 241-243.
- (S2) E. Kowalska, O. O. P. Mahaney and B. Ohtani, Visible-light-induced photocatalysis through surface plasmon excitation of gold on titania surfaces. *Phys. Chem. Chem. Phys.*, 2010, **12**, 2344-2355.
- (S3) K. Kimura, S. Naya, Y. Jin-nouchi and H. Tada, TiO<sub>2</sub> crystal form-dependence of the Au/TiO<sub>2</sub> plasmon photocatalyst's activity. *J. Phys. Chem. C*, 2012, **116**, 7111-7117.
- (S4) S. Naya, K. Kimura and H. Tada, One-step selective aerobic oxidation of amines to imines by gold nanoparticle-loaded rutile titanium(IV) oxide plasmon photocatalyst. *ACS Catalysis*, 2013, **3**, 10-13.
- (S5) J. B. Priebe, J. Radnik, A. J. J. Lennox, M.-M. Pohl, M. Karnahl, D. Hollmann, K. Grabow, U. Bentrup, H. Junge, M. Beller and A. Bruckner, Solar hydrogen production by plasmonic Au-TiO<sub>2</sub> catalyst: impact of synthesis protocol and TiO<sub>2</sub> phase on charge transfer efficiency and H<sub>2</sub> evolution rates. *ACS Catal.*, 2015, **5**, 2137-2148.
- (S6) S. Naya, T. Niwa, T. Kume and H. Tada, Visible-light-induced electron transport from small to large nanoparticles in bimodal gold nanoparticle-loaded titanium(IV) oxide. *Angew. Chem. Int. Ed.*, 2014, **53**, 7305-7309.
- (S7) S. Wang, Y. Gao, S. Miao, T. Liu, L. Mu, R. Li, F. Fan and C. Li, Positioning the water oxidation reaction sites in plasmonic photocatalysts. *J. Am. Chem. Soc.*, 2017, **139**, 11771-11778.

- (S8) T. Onishi, M. Teranishi, S. Naya, M. Fujishima and H. Tada, Electrocatalytic effect on the photon-to-current conversion efficiency of gold-nanoparticle-loaded titanium(IV) oxide plasmonic electrode for water oxidation. *J. Phys. Chem. C*, 2020, **124**, 6103-6109.
- (S9) S. Naya, T. Nikawa, K. Kimura and H. Tada, Rapid and complete removal of nonylphenol by gold nanoparticle/rutile titanium(IV) oxide plasmon photocatalyst. *ACS Catal.*, 2013, **3**, 903-907.
- (S10) S. Naya and H. Tada, Dependence of the plasmonic activity of Au/TiO<sub>2</sub> for the decomposition of 2-naphthol on the crystal form of TiO<sub>2</sub> and Au particle size. *J. Catal.*, 2018, **364**, 328-333.

**Table S2.** Characterization results of the Au/A-TiO<sub>2</sub> and Au/R-TiO<sub>2</sub> plasmonic photocatalysts.

Catalysts	$d_{\text{Au}} / \text{nm}$ (counts)	$x_{\text{Au}} / \text{mass\%}$	Faceting probability / % (counts)	$T_c / \text{K}$	$t_c / \text{h}$
Au/A-TiO <sub>2</sub>	3.5 ± 0.9 (203)	4.25	negligible (1032)	673	1
Au/A-TiO <sub>2</sub>	4.1 ± 0.8 (208)	4.20	negligible (1045)	673	4
Au/A-TiO <sub>2</sub>	5.0 ± 0.9 (205)	4.21	negligible (1021)	773	4
Au/A-TiO <sub>2</sub>	6.6 ± 1.4 (208)	4.24	0.1 (1032)	873	4
Au/A-TiO <sub>2</sub>	7.9 ± 1.6 (209)	4.21	0.2 (1037)	873	24
Au/R-TiO <sub>2</sub>	3.6 ± 1.1 (210)	4.22	14.1 (1017)	673	1
Au/R-TiO <sub>2</sub>	4.0 ± 0.9 (211)	4.16	3.6 (1013)	673	4
Au/R-TiO <sub>2</sub>	5.1 ± 1.0 (213)	4.21	1.8 (1009)	773	4
Au/R-TiO <sub>2</sub>	7.5 ± 1.9 (213)	4.31	0.9 (1037)	873	4
Au/R-TiO <sub>2</sub>	10.0 ± 2.2 (204)	4.19	0.8 (1019)	873	24
Au/R-TiO <sub>2</sub> NR	3.5 ± 0.7 (223)	4.20	94.2 (1029)	673	1
Au/R-TiO <sub>2</sub> NR	6.3 ± 1.1 (205)	4.18	88.7 (1034)	873	24

**Table S3.** Au 4f and Ti 2p-XP binding energies

Samples	$d_{\text{Au}}$ / nm	Au		Ti	
		$4f_{7/2}$ / eV	$4f_{5/2}$ / eV	$2p_{3/2}$ / eV	$2p_{1/2}$ / eV
A-TiO <sub>2</sub>	---	---	---	458.3	464.0
Au/A-TiO <sub>2</sub>	3.5 ± 0.9	83.3	87.0	458.7	464.4
Au/A-TiO <sub>2</sub>	4.1 ± 0.8	83.2	86.9	458.6	464.3
Au/A-TiO <sub>2</sub>	5.0 ± 0.9	83.1	86.8	458.5	464.3
Au/A-TiO <sub>2</sub>	6.6 ± 1.4	83.0	86.7	458.5	464.3
Au/A-TiO <sub>2</sub>	7.9 ± 1.6	83.2	86.9	458.7	464.3
R-TiO <sub>2</sub>	---	---	---	458.3	464.2
Au/R-TiO <sub>2</sub>	3.6 ± 1.1	83.2	86.9	458.4	464.3
Au/R-TiO <sub>2</sub>	4.0 ± 0.9	83.3	87.0	458.6	464.3
Au/R-TiO <sub>2</sub>	5.1 ± 1.0	83.2	86.9	458.4	464.3
Au/R-TiO <sub>2</sub>	7.5 ± 1.9	83.2	86.9	458.5	464.2
Au/R-TiO <sub>2</sub>	10.0 ± 2.2	83.1	86.7	458.4	464.2

**Table S4.** Comparison of the local electric field between HS Au/A-TiO<sub>2</sub> and t-O<sub>h</sub> Au/R-TiO<sub>2</sub> systems calculated by the 3D-FDTD method

Model	$d_{\text{Au}} / \text{nm}$	$\lambda / \text{nm}$	Monitor plane	Maximum E / E <sub>0</sub>	Maximum  E  <sup>2</sup> /  E <sub>0</sub>   <sup>2</sup>
HS Au/A-TiO <sub>2</sub>	3.5	702	$xz$	49.6	2.5E+03
			$xy$	59.9	3.6E+03
t-O <sub>h</sub> Au/R-TiO <sub>2</sub>	3.6	675	$xz$	138	1.9E+04
			$xy$	382	1.5E+05
		704	$xz$	272	7.4E+04
			$xy$	453	2.1E+05
		722	$xz$	448	2.0E+05
			$xy$	448	2.0E+05